Digestive Diseases and Sciences (2019) 64:1257–1269
https://doi.org/10.1007/s10620-018-5398-4

ORIGINAL ARTICLE

Nonalcoholic Fatty Liver Disease Demonstrates a Pre-fibrotic and Premalignant Molecular Signature

Diego Almanza[1,2] · Mehrnaz Gharaee-Kermani[1,2] · Alisa Zhilin-Roth[1,2] · Jose A. Rodriguez-Nieves[2] · Cory Colaneri[1] · Todd Riley[1,2] · Jill A. Macoska[1,2]

Received: 30 August 2017 / Accepted: 27 November 2018 / Published online: 5 December 2018

Abstract

Background Metabolic syndrome contributing to nonalcoholic fatty liver disease (NAFLD) can lead to hepatic dysfunction, steatohepatitis, cirrhosis, and hepatocellular carcinoma.

Aims In this study, we tested whether diet-induced fatty liver in a mouse model physiologically mimicked human NAFLD, and whether transcriptional alterations in mouse fatty liver signified risk for the development of hepatitis, cirrhosis, and/or hepatocellular carcinoma.

Methods SAMP6 strain mice were fed a low-fat diet or high-fat diet (HFD) for 6 months. Mouse livers were isolated and subjected to histology, immunohistochemistry, and whole transcriptome RNA sequencing. Sequences were aligned to the mouse reference genome, and gene expression signatures were analyzed using bioinformatics tools including Cufflinks, Pathview, Cytoscape, ClueGO, and GOstats.

Results Consistent with NAFLD, livers from HFD-fed mice demonstrated steatosis, high levels of inflammation, an up-regulation of genes encoding proteins associated with the complement pathway and immune responses, and down-regulation of those associated with metabolic processes. These livers also showed an up-regulation of genes associated with fibrosis and malignant transformation but no histological evidence of either pathobiology or DNA damage.

Conclusions HFD-fed mice exhibited NAFLD that had incompletely transitioned from fatty liver to NASH. Importantly, bioinformatics approaches identified pre-fibrotic and premalignant signatures, suggesting that the pathogenesis of both fibrosis and cancer may initiate in fatty livers well before associated histological changes are evident.

Keywords NAFLD · Fibrosis · Cancer · Diet

Introduction

Metabolic syndrome, a spectrum disorder defined by high blood pressure, high body mass index/abdominal circumference, glycemia, triglyceridemia, proinflammatory state, and high HDL cholesterol concentrations, has increased concurrent with obesity in the American population [1–4]. In particular, nonalcoholic fatty liver disease (NAFLD), cirrhosis, and ultimately hepatocellular carcinoma can be consequent to many of the pathobiology associated with metabolic syndrome [4]. NAFLD has become one of the most common liver diseases and an estimated 20–30% of individuals in the Western population are diagnosed with NAFLD and suffer from liver-related morbidity and mortality [1, 5]. Histologically, NAFLD is characterized by steatosis, e.g., fat accumulation. Fatty liver with demonstrable inflammation, DNA damage, and some degree of fibrosis is considered nonalcoholic steatohepatitis (NASH) [6]. Quantification of the hepatocytes containing fat droplets in the liver can give an indication into the severity of the steatosis, and the recommended lower threshold has been set to 5% of the liver mass being composed of hepatocytes containing fat [7].

Electronic supplementary material The online version of this article (https://doi.org/10.1007/s10620-018-5398-4) contains supplementary material, which is available to authorized users.

✉ Jill A. Macoska
Jill.Macoska@umb.edu

[1] Department of Biology, University of Massachusetts Boston, Boston, USA

[2] Center for Personalized Cancer Therapy, The University of Massachusetts Boston, Room 4601, Integrated Sciences Complex, 100 Morrissey Blvd., Boston, MA 02125, USA

In order to better understand the relationship between obesity and downstream organ pathobiologies, we have developed a mouse model of diet-induced obesity that successfully mimics several aspects of metabolic syndrome. This model employs senescence-accelerated mouse prone 6 (SAMP6) mice, an inbred strain of AKR/J mice that exhibit an accelerated aging phenotype [8]. SAMP6 and AKR/J mice fed a high-fat diet (HFD) for 6 months developed insulin resistance, hyperglycemia, obesity, urinary voiding dysfunction, and fatty livers [9]. In the current study, we hypothesized that the fatty livers of the HFD-fed mice mimicked human NAFLD. Therefore, we determined whether these mice might provide a good model to study the chronology of transcriptional changes that potentially drive the development of NAFLD. These studies showed that livers from HFD-fed mice demonstrated steatosis, inflammation, an up-regulation of genes encoding proteins associated with the complement pathway and immune responses, down-regulation of those associated with metabolic processes, and little DNA damage. Therefore, the transcriptome signatures of the fatty livers from the HFD-fed SAMP6 mice were consistent with that of NAFLD that had incompletely transitioned from fatty liver to NASH. Surprisingly, the fatty livers also showed an up-regulation of genes associated with extracellular matrix deposition and malignant transformation, but no histological evidence of fibrosis or hepatocellular carcinoma. Therefore, the NAFLD livers expressed a pre-fibrotic and premalignant signature in the absence of any other indication of either fibrosis or cancer.

Materials and Methods

Mouse Strains and Husbandry

The senescence-accelerated mouse prone 6 (SAMP6) mouse strain was used in this study (Harlan Laboratories, Indianapolis, IN) [8]. Senescence-accelerated mouse (SAM) models have been developed by selective sister–brother breeding of the AKR/J strain and now comprise 12 lines: senescence-prone inbred (SAMP) strains 1, 2, 3, 6, 7, 8, 9, 10, and 11, and senescence-resistant (SAMR) strains 1, 4, and 5 [10]. The pathobiologies of these mice differ widely, though the SAMP6 strain is characterized by amyloidosis, osteoporosis, and prostatic fibrosis [10–12]. Genetically, SAMP6 mice carry a mutant Abcb1a allele common to many of the SAMP strains, as well as a p.S540fs frameshift mutation in the Il4ra gene potentially associated with ulcerative colitis and osteoporosis [13, 14]. The rationale for using the SAMP6 mouse strain is based on our observation of the development of fatty liver in mice fed a high-fat diet, and lack of genetic predisposition for this pathobiology [9]. Additionally, the accelerated aging phenotype facilitates response to a high-fat diet (which can be difficult to tolerate over extended periods of time) such that these mice demonstrate pronounced fatty liver and a metabolic syndrome phenotype, e.g., obesity, hyperglycemia, and insulin resistance, consistent with human type 2 diabetes, after 6 months on the diet [9]. For these studies, mice were put on the following diets at 6–8 weeks of age: high-fat diet (HFD) containing 60% calories from fat, 20% protein, and 20% carbohydrates (58Y1, Test Diet, Richmond, IN) or low-fat diet (LFD) containing 10.2% calories from fat, 18.3% protein, and 71.5% carbohydrates (58Y2, Test Diet, Richmond, IN). These chows are considered "paired" diets by the manufacturer and are intended to be used in tandem for diet-induced obesity (DIO) studies [15]. The mice were fed daily with fresh high- or low-fat chow (5 g/day) for 6 months [9]. Mice were housed in the vivarium facility at the University of Massachusetts Boston under enriched conditions at a constant temperature (22–23 °C) with a 12/12-h light/dark cycle and optimal humidity and free access to tap water and food ad libitum. Upon completion of the studies, mice were killed and a portion of the liver tissues snap-frozen in liquid nitrogen and stored at − 80 °C, while another portion was fixed and paraffin-embedded. All animal procedures were performed using protocols approved by the Institutional Animal Care and Use Committee (IACUC).

Immunohistochemistry

Formalin-fixed paraffin-embedded tissue sections of 5 μM were deparaffinized using reagents and protocols from the manufacturer (HistoClear, Thermo Fisher Scientific, Waltham, MA). Antigen retrieval and immunohistochemistry were performed as described previously using HistoFine Simple Stain AEC Solution (Nichirei Biosciences, Tokyo, Japan) and Harris hematoxylin solution counterstain (Sigma-Aldrich) [16] and goat anti-mouse CD8 antibody (Abcam, ab203035). For positive control, mouse spleen sections were incubated with anti-CD8 primary and anti-rabbit secondary antibodies; for negative control, mouse spleen sections were incubated with anti-rabbit secondary antibody only. CD8 expression levels were assessed on whole tissue sections using ImmunoMembrane [17].

TUNEL Staining

TUNEL staining for the detection of apoptotic cells was accomplished using reagents and protocols from the manufacturer (Roche In Situ Cell Detection Kit). The tissue sections were pre-incubated with DEPC to prevent proteinase K-mediated activation of DNAseI and consequent high numbers of false-positive apoptotic nuclei [18]. As a positive control, sections of normal mouse liver were microwaved for 20 min to induce DNA damage; as a negative control, other

sections were incubated, fixed, and permeabilized without exposure to proteinase K.

Collagen Content

Collagen content was determined using Masson's trichrome-stained tissue sections as described previously [9]. The stained tissue sections were digitally imaged using a PathScan Enabler IV and color segmented using a subprogram within MATLAB (R2010a; MathWorks, Natick, Mass) which separates and quantifies color elements from trichrome images, permitting quantitation of blue-stained areas corresponding to extracellular collagen. Using the area of a single tissue section as the denominator, this approach provides a means to calculate the portion of this area that is made up by mature extracellular collagen I (the numerator), hence the percentage of extracellular collagen type I (numerator/denominator × 100) in that tissue section. By extension, this method also permits calculation of the percentage of the entire piece of tissue that is made up of mature extracellular collagen I [9].

Tissue Homogenization and RNA Preparation

One hundred milligrams of frozen tissue was disrupted in 1 mL TRIZOL reagent (Invitrogen, Carlsbad, CA) using an electric homogenizer until the tissue was completely dissolved in solution. Once homogenized, aliquots of the solution were transferred to Eppendorf tubes and left in TRIZOL at room temperature for 5 min. Phase separation was then performed using 200 µl chloroform for 15 s and left at room temperature for 5 min. Samples were then centrifuged at 12000*g* for 15 min at 2–8 °C. The aqueous phase (top) was transferred to a fresh RNAse-free tube and RNA precipitated with isopropanol. RNA pellets were collected via centrifugation, washed, resuspended, reprecipitated, suspended in 50 µl DEPC water, and stored at − 80 °C until use.

Library Preparation and Sequencing

Libraries were prepared from RNA isolated from three HFD-fed and three LFD-fed SAMP6 mice. Total RNA samples were DNAse-treated, and 300 ng was used as input to create single-indexed (six base pairs) RNASeq libraries using the TruSeq RNA preparation kit according to the manufacturer's protocol (Illumina, Carlsbad, CA). Samples were pooled together and sequenced on a two-lane flow cell using onboard cluster generation with the Illumina HiSeq™ 2500 instrument. A 51-cycle paired-end rapid run of the single-indexed RNASeq libraries was performed. Raw data of the Bcl base call files were then demultiplexed upon completion.

Bioinformatics Analysis

Bcl base call files were converted to FASTQ format using Illumina's bcl2fastq conversion tool v1.8.4. Stringent conversion parameters were set by not allowing a mismatch in the index during the demultiplexing process. Additionally, FASTQ files were created overwriting the default parameter to split the files after 4 million reads, generating a single FASTQ file for each sample replicate. Alignment of reads was carried out using Tophat v2.0.14 post-FASTQ file conversion using Illumina's bcl2fastq tool v1.8.4 [19, 20]. Alignment parameters for Tophat consisted of utilizing the default parameters, which were sufficient for downstream analysis of data. The reference genome file used for the alignment was the mm10 Genome Reference Consortium GRCm38.p4, and the gene transcript file was provided by iGenomes (Illumina, Carlsbad, CA) [21]. Cufflinks v2.2.1 was used to estimate the relative abundance of transcripts aligned for all the samples [22]. Cuffdiff v2.2.1 was used to perform the differential gene expression analysis post-quantification of the transcripts for the samples [23]. EdgeR analysis of gene transcripts differentially expressed by the livers of HFD-fed and LFD-fed mice was performed using the empirical analysis of digital gene expression data in R (edgeR) using a statistical cutoff and was set to p value ≤ 0.001 [24]. The edgeR table for genes demonstrating ≥ 2 or ≤ 2 fold difference between HFD-fed and LFD-fed mice is provided in Supplementary Table I.

Gene set enrichment analysis using Pathview v1.10.1 was used to elucidate the top cellular pathways that are overall up-regulated, or down-regulated by HFD compared to LFD [25]. In addition, selected pathways of interest were also picked for visualization of the overall regulation of the pathways. The statistical cutoff was set to a q value ≤ 0.05. Network analysis of the differential expression analysis was accomplished using Cytoscape v3.3.0 [26]. Gene sets of twofold or higher up-regulated genes in HFD mice, and 0.1–0.5-fold lower down-regulated genes in the HFD mice with a p value cutoff of 0.05 was used as the gene set entry for the network analysis of the mouse interactome. Interactomes used for this analysis were provided by the Cytoscape program, loaded with the mouse interactome from BioGRID database release 3.4.129.

Gene ontology analysis of the gene sets, both twofold or higher up-regulated genes in HFD mice and 0.1–0.5-fold lower down-regulated genes in the HFD mice, was performed using ClueGO and GOstats. ClueGO v2.2.3 was used for the analysis of the two sets of genes, both up-regulated and down-regulated genes in the HFD mice [27]. GOstats v2.36.0 was used to assess biological processes associated with genes differentially in the livers of the HFD-fed and LFD-fed mice [28]. Statistical cutoff for both computational programs was set to a p value of ≤ 0.05.

NanoString Quantitation of RNA Transcripts

NanoString nCounter™ Mouse Inflammation v2 panel consisting of 248 inflammation-related mouse genes and six internal reference genes was interrogated using the same total RNA isolated from the liver tissues. Hundred nanograms of input total RNA was used in the hybridization reactions as recommended in the NanoString's nCounter™ Gene Expression Assay Manual (NanoString Technologies, Seattle, WA). After hybridization, data were collected by the nCounter Prep Station v4.1.0.1 and nCounter Digital Analyzer v3.1.0.1. Raw nCounter data were analyzed using the nSolver analysis software v2.5.34. Normalization of the data was carried out in two different steps. First using the geometric mean of the positive controls probes provided by NanoString, the data were normalized to this prior to normalization using the housekeeping probes. Normalized data, and genes with counts higher than 10 were then used for the rest of the analysis. All statistical significance was set to a p value of ≤ 0.05.

Results

Liver Histology and Phenotyping

We have previously reported that HFD-fed SAMP6 mice developed enlarged livers after 6–8 months on the diet [9]. This was also apparent in the current study, and all three HFD-fed mice exhibited liver steatosis (Fig. 1b, f–h) though this was not evident in livers from LFD-fed mice (Fig. 1a, c–e). Carcinoma was not observed in the liver tissues of either HFD- or LFD-fed mice (Fig. 1). The assessment of collagen content from Masson's trichrome-stained slides demonstrated less than 1% collagen content and no significant differences in collagen content between the livers of HFD- and LFD-fed mice ($p = 0.39$).

In order to delineate whether the observed fatty livers in HFD-fed mice comprised nonalcoholic fatty liver (NAFL) or nonalcoholic steatohepatitis (NASH), the livers were examined for the evidence of hepatic steatosis plus hepatocyte injury and inflammation, which are characteristic of NASH but not NAFL [29]. Inflammation, particularly elevated levels of CD8+ T lymphocytes, is a marker of liver damage associated with NASH [30, 31]. As noted above, inflammation was evident in liver tissues from HFD-fed, but not LFD-fed mice (Fig. 1). Immunohistochemical analysis demonstrated high levels of CD8+ protein expression in liver tissues from HFD-fed mice (average 3+ staining) (Fig. 2a, b) which appeared similar to mouse spleen stained for CD8 (positive control) (Fig. 2g). In contrast, liver tissues from LFD-fed mice (average 2+ staining) (Fig. 2c, d) evidenced little or no staining similar to mouse spleen stained with anti-rabbit secondary antibody only (negative control) (Fig. 2h). CD8 staining was significantly higher in liver tissues from HFD-compared the LFD-fed mice ($p < .001$) (Fig. 2). Apoptosis was evaluated using TUNEL staining (Fig. 2e, f). Enumeration of these nuclei revealed very low (< 2%) apoptotic rates similar to those observed for negative control (non-proteinase K-treated mouse liver) (Fig. 2j) rather than positive control (microwaved mouse liver tissue) (Fig. 2i), and did not demonstrate statistically significant differences in the number of apoptotic nuclei.

Given these observations, we assessed that the HFD-fed mouse fatty livers were consistent with NAFLD that

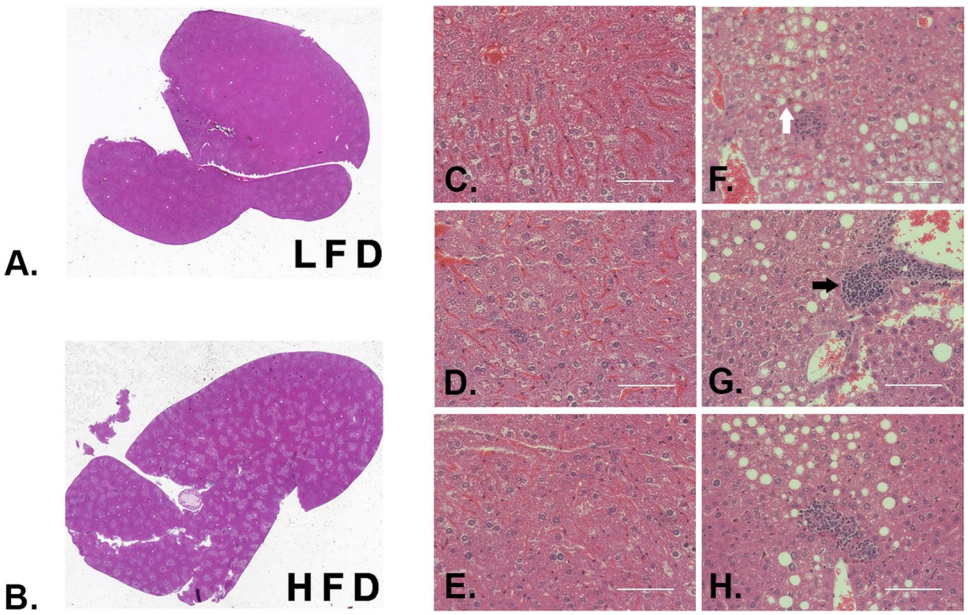

Fig. 1 Liver pathology of HFD- and LFD-fed mice. Photomicrographs of hematoxylin/eosin-stained sections from LFD-fed mice (**a**) and HFD-fed mice (**b**) at 4× magnification, and of the three LFD-fed mice (**c**–**e**) and three HFD-fed mice (**f**–**h**) used in the sequencing studies at 40× magnification. Steatosis is evident in sections from HFD- (**f**–**h**) but not LFD-fed mice (**c**–**e**) (example indicated by white arrow in **F**). Inflammation is also evident in sections from HFD- (**f**–**h**) but not LFD-fed mice(**c**–**e**) (example indicated by black arrow in **g**)

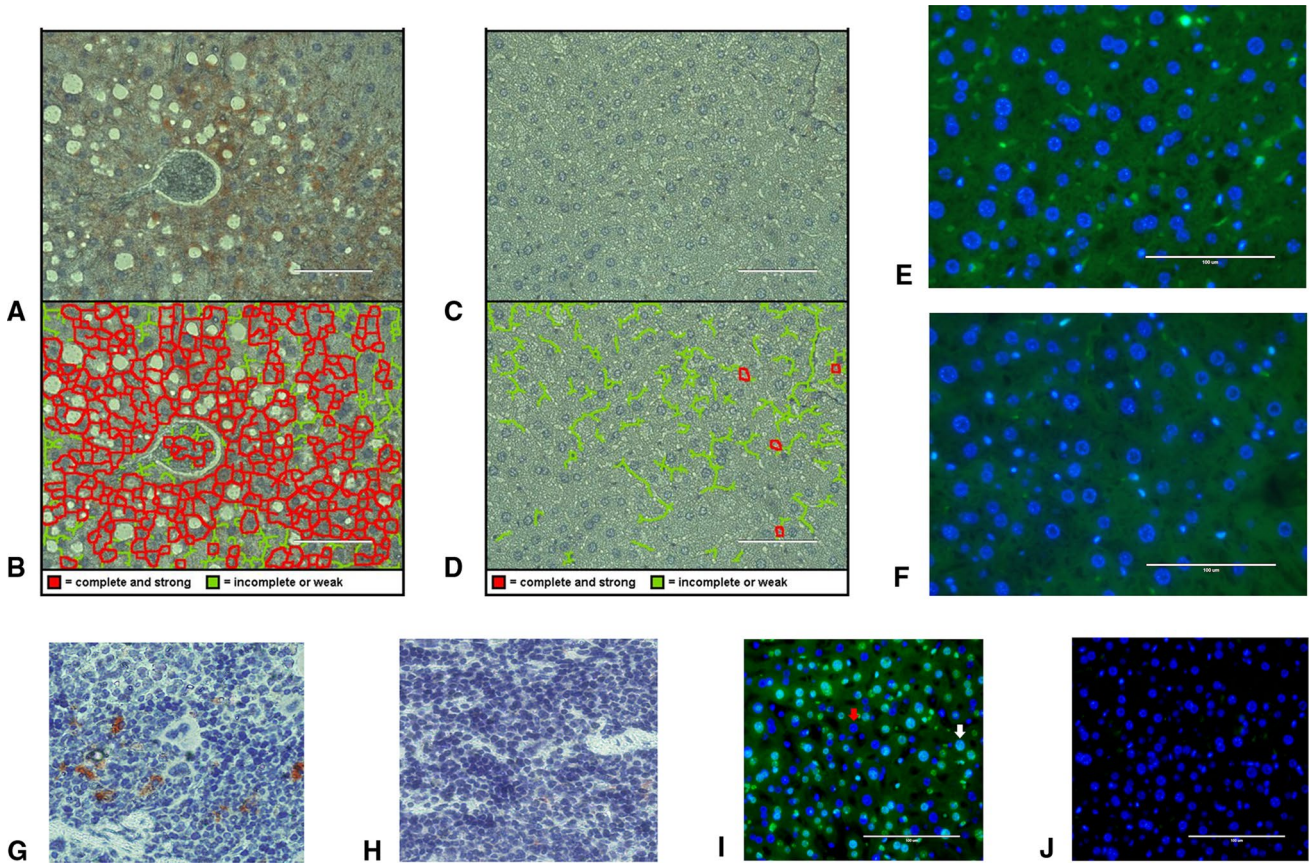

Fig. 2 Fatty liver phenotyping reveals high levels of inflammatory infiltrate and low apoptotic index. **a**–d, **g**, **h** CD8 staining. Fixed sections of liver tissue from HFD- and LFD-fed mice were probed for CD8 protein, counterstained with hematoxylin **(a, c),** and analyzed for CD8 content (**b**, **d**). Red, complete/strong staining; green, incomplete/weak staining. Liver sections from HFD-fed mice demonstrated significantly higher ($p < .0001$) CD8 protein expression compared to LFD-fed mice. **g** Mouse spleen stained with anti-CD8 primary antibody and anti-rabbit secondary antibody (positive control); **h** mouse spleen stained with anti-rabbit secondary antibody only (negative control). Photomicrographs taken at 40× magnification. **e**, **f**, **i**, **j** TUNEL staining. Fixed sections of liver tissue from HFD-fed (**e**) and LFD-fed mice (**f**) were assessed for apoptosis using TUNEL staining. The number of apoptotic nuclei was not significantly different between fatty and lean liver tissues. **i** Positive control: section of normal mouse liver microwaved for 20 min to induce DNA damage; red arrow points to non-apoptotic nucleus (dark blue), and white arrow points to apoptotic nucleus (aqua). **j** Negative control: section of normal mouse liver treated as in **e** and **f** without exposure to proteinase K. Photomicrographs taken at 40×

exhibited inflammation, but little DNA damage, therefore, had incompletely transitioned from fatty liver to NASH [31].

NAFLD Transcriptome

Differential gene expression analysis of RNA purified from the livers of HFD- and LFD-fed mice demonstrated 2067 differentially expressed transcripts at the $p < .001$ significance level and false discovery rate < 5%. These data were assessed at the gene set level in order to determine what processes or gene ontology the transcripts were regulating. In order to ensure stringency, this analysis was confined to the examination of transcripts that were ≥ twofold up-regulated or ≥ twofold down-regulated in liver RNA from HFD-fed compared to LFD-fed mice (Supplementary Table I). Principle components analysis (PCA) of the molecular signatures of livers from HFD- and LFD-fed mice demonstrated significant separation associated with diet (Fig. 3a). Gene ontology analysis using ClueGO revealed that processes related to immune responses were highly up-regulated (Fig. 3b), whereas metabolic processes were greatly down-regulated (Fig. 3c), in the HFD-fed compared to LFD-fed mouse liver transcriptomes. The up-regulation of immune response genes is consistent with the observed significantly higher levels of immune cells observed in the fatty livers (Figs. 1, 2) and suggests that metabolic syndrome-induced inflammation promoted NAFLD development in the HFD-fed mice. Conversely, the pronounced down-regulation of genes that function in multiple metabolic processes may indicate the general hepatic dysfunction consequent to NAFLD. Taken all together, these data indicate high levels

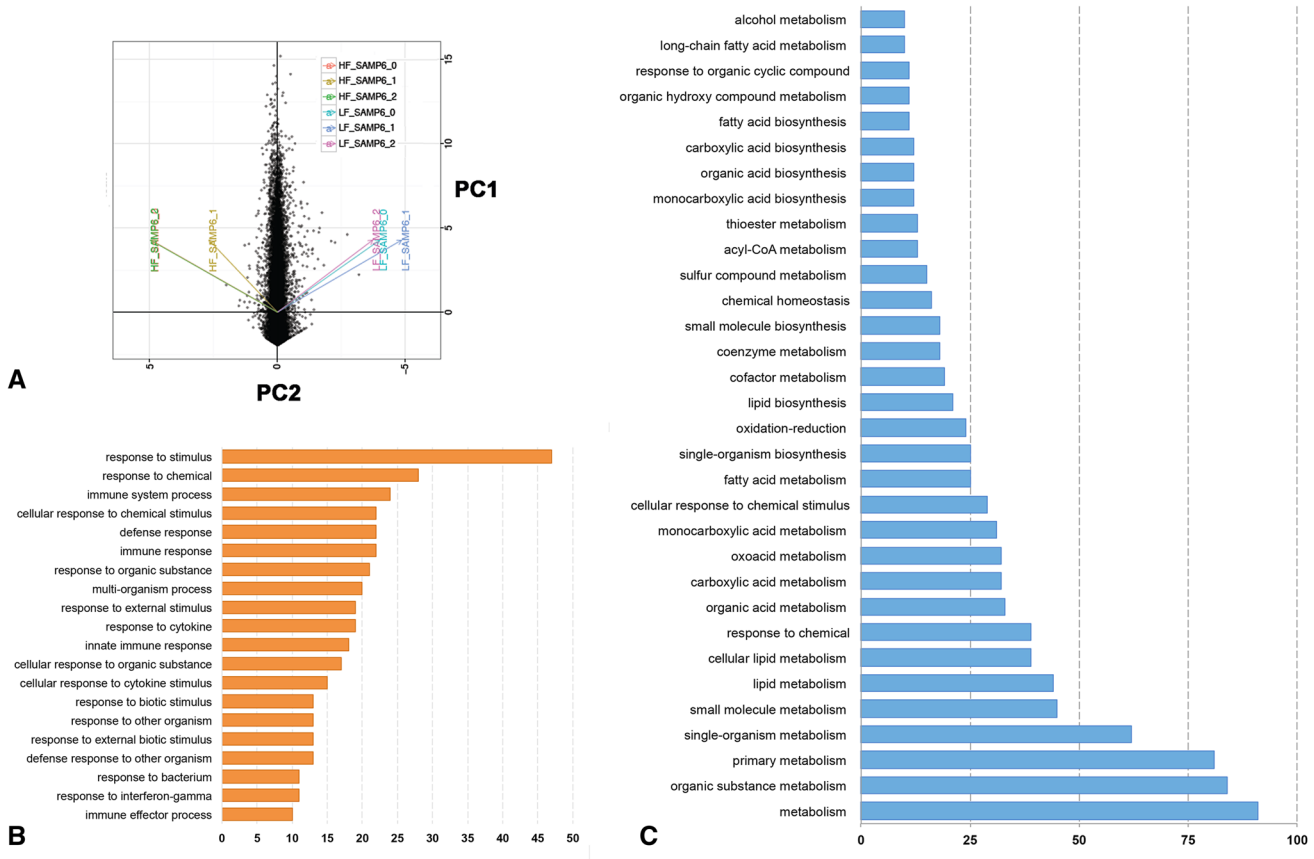

Fig. 3 Principle components and gene ontology analysis of molecular signatures of HFD- and LFD-fed mice**. a** Principle components analysis (PCA) of differential gene expression (DGE) patterns of high-fat diet-fed (HFD) and low-fat diet-fed mice (LFD) demonstrate significant separation associated with diet. Three mice (0, 1, and 2) per diet were assessed. **b**. Gene ontology analysis shows that biological processes related to immune responses were highly up-regulated in the livers of HFD-fed compared to LFD-fed mice. **c** Gene ontology analysis of biological processes shows that those related to metabolic functions were highly down-regulated in the livers of HFD-fed compared to LFD-fed mice. Axes show number of gene counts in each process category

of metabolic syndrome-promoted changes in gene transcription profiles associated with NAFLD.

Use of the Pathview tool identified several key molecular, cellular, and metabolic pathways affected by obesity-induced transcriptomic changes in the livers of HFD-fed mice. Figure 4a shows the top significant (p value ≤ 0.05) pathways that were up-regulated in the livers of HFD-fed mice. Notably, "Complement and Coagulation Cascades" was the top significant up-regulated pathway, and several genes that encode proteins in this pathway were significantly up-regulated in the livers of HFD-fed compared to LFD-fed mice (Fig. 4b). This is consistent with several studies showing that the complement system, which mediates inflammation, is up-regulated and activated, and serves as biomarkers, in human NAFLD [32–35]. Moreover, complement factor 3 (C3) is specifically indicative of high liver fat content and liver enzymes, including aspartate amino transferase (AST), alanine aminotransferase (ALT), and γ-glutamyl transferase (GGT) [35, 36]. In addition, two of the pathways up-regulated in the livers of HFD-fed mice are part of the immune response, consistent with the gene ontology data shown in Fig. 3b.

Validation of RNASeq Data

A NanoString nCounter mRNA inflammation panel was interrogated to validate the HiSeq transcript-level expression data as shown in the NanoString nCounter data correlated well with the Illumina HiSeq data. Although the absolute levels of gene transcript levels observed were not identical, the direction of gene transcript level, e.g., up- or down-regulated, was the same using the two approaches. For example, the fold change transcript level for the *Cd4* gene was twofold higher measured by nCounter and 1.4-fold higher measured by RNASeq in livers from HFD- than LFD-fed mice (Fig. 5a). Similarly, the fold change transcript level for the *Tlr5* gene was 0.6-fold lower measured by nCounter and − 1.1-fold lower measured by RNASeq

A

KEGG Pathview ID	Pathway Name	greater.p.val	greater.q.val
mmu04610	Complement and coagulation cascades	2.21E-08	4.56E-06
mmu04612	Antigen processing and presentation	1.69E-07	1.75E-05
mmu04514	Cell adhesion molecules (CAMs)	8.89E-06	0.000610158
mmu04145	Phagosome	8.37E-05	0.004308377
mmu04623	Cytosolic DNA-sensing pathway	0.000317954	0.013099719
mmu04380	Osteoclast differentiation	0.000984612	0.033805001
mmu04650	Natural killer cell mediated cytotoxicity	0.003006892	0.088488541

B

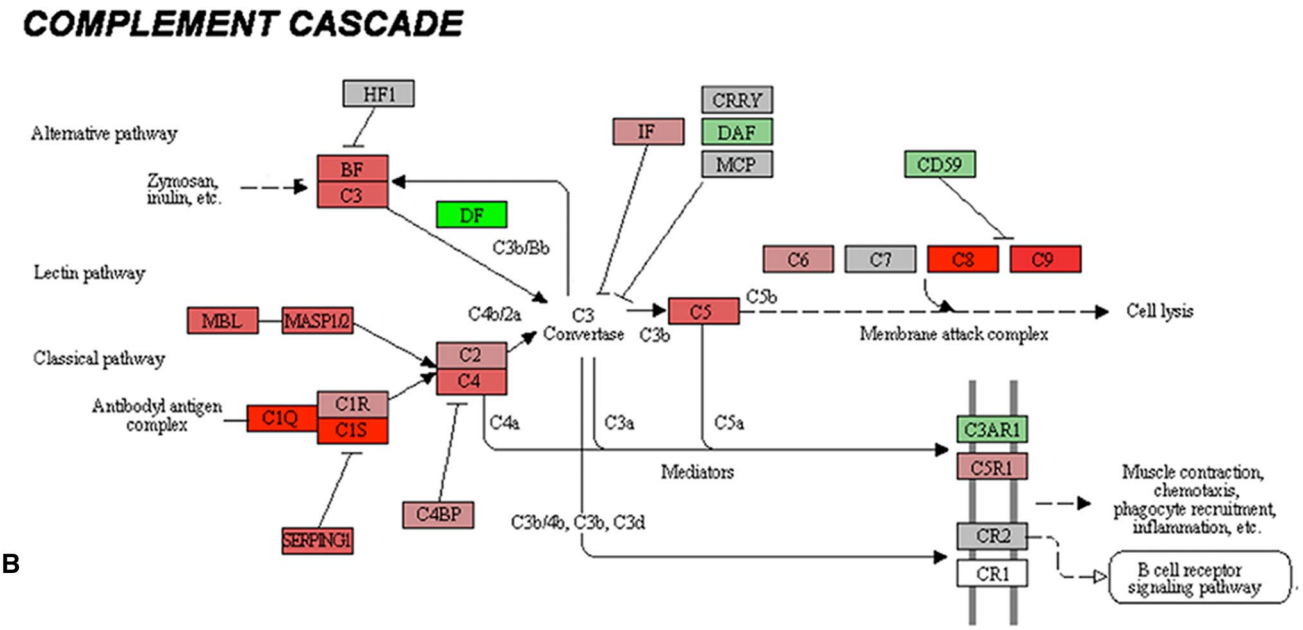

Fig. 4 KEGG Pathview analysis of molecular signature of HFD-fed mice. **a** Top significant up-regulated pathways in HFD-fed compared to LFD-fed mice demonstrate up-regulation of complement and immune-related pathways. **b** KEGG pathway analysis demonstrating up-regulation of multiple components of the complement pathway

in livers from HFD- than LFD-fed mice (Fig. 5b). Notably, genes that are members of complement family (C1s, C3, C1ra, C8a, C4a, C8b, C6, C2, indicated by asterisk in Fig. 5a) were up-regulated in RNA purified from the livers of HFD- compared to LFD-fed mice. This further demonstrates the congruence of data obtained using RNASeq and nCounter analysis and also validates the KEGG Pathview analysis of the RNASeq data that indicated the significance of the complement and coagulation cascades in mouse fatty liver (Fig. 4) [32, 34]. Several recent studies have shown that the complement system is elevated in NAFLD and that C3 may serve as a serum marker for fatty liver disease [36]. The observation that several genes encoding complement proteins are up-regulated in fatty livers from the HFD-fed mice demonstrates that this obesity-based mouse model closely mimics human NAFLD.

Premalignant and Pre-cirrhotic Gene Signatures Associated with Diet-Induced NAFLD

If not treated in time or left untreated, NAFLD can progress to cirrhosis and hepatocellular carcinoma (HCC). Several biomarkers have been associated with HCC; therefore, we examined the fatty liver RNA sequencing dataset for the presence of gene transcripts correlative to these known biomarkers in mice. As shown in Fig. 6, RNA from the livers of HFD-fed mice demonstrates up-regulation of transcripts encoding signaling proteins associated with HCC, including those mediated by G-protein-coupled receptor (GPCR) activation or involved in Wnt, PI3 K/NFkB, and MEK/ERK signaling [37–39]. In addition, our group also observed a strong transcriptional up-regulation of genes encoding extracellular matrix proteins in the livers of HFD-fed mice (Fig. 7). Up-regulation ECM proteins are consequent to

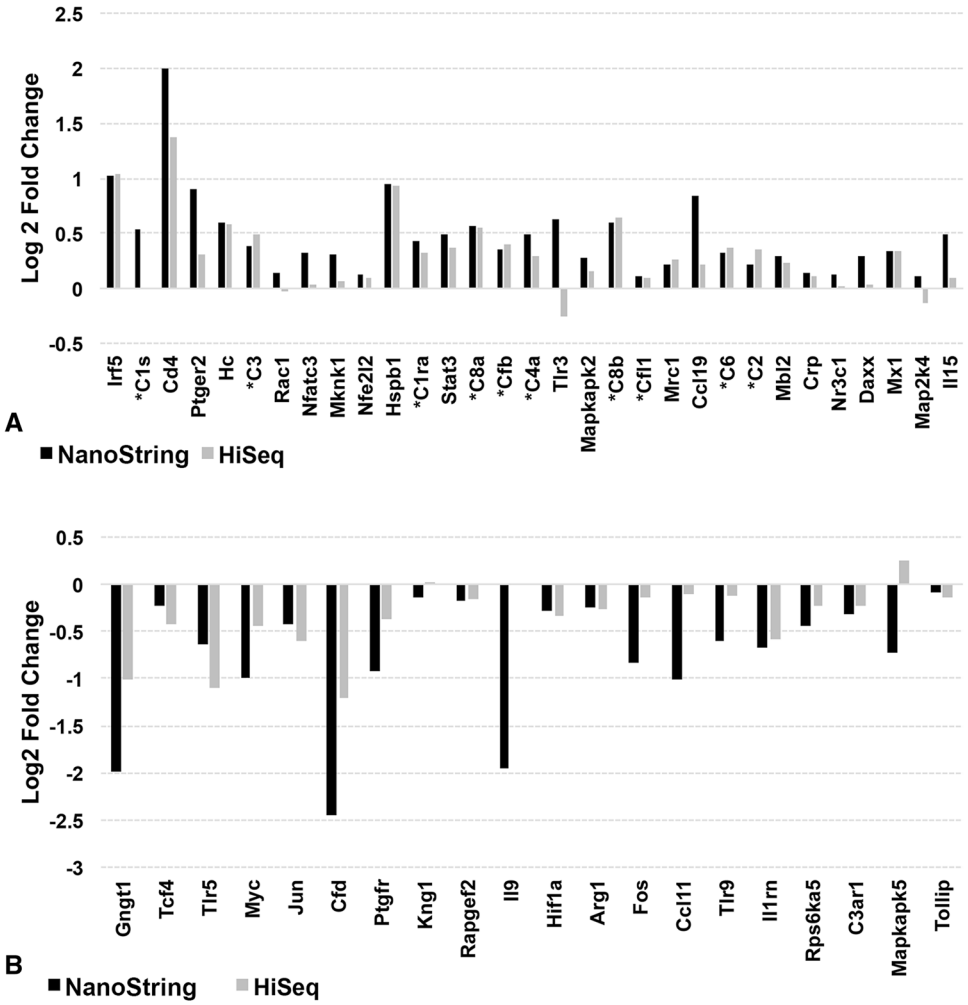

Fig. 5 NanoString nCounter evaluation of fatty liver molecular signature. RNA prepared from three HFD-fed and three LFD-fed livers was interrogated using the NanoString nCounter Mouse Inflammation v2 panel consisting of 248 inflammation-related mouse genes. The graph of fold HFD/LFD transcript levels from the NanoString data (black bars) and that from the HiSeq data (gray bars) shows that, although the absolute levels of gene transcript levels observed were not identical, the "trend" in gene transcript level, e.g., up- or down-regulated, was the same using the two approaches. Transcripts from multiple complement pathway genes (indicated by asterisk *) were up-regulated in the livers of HFD-fed mice using both approaches

fibrosis, which, in the liver, can advance to cirrhosis [40–42]. Neither the HFD-fed or LFD-fed mice demonstrated histological liver fibrosis. This finding suggests that a pre-fibrotic signature is evident in the livers of the HFD-fed mice. Taken together, these observations suggest that the fatty livers of HFD-fed mice harbor both premalignant and pre-fibrotic gene signatures, suggesting that these signatures signal the initiation of these pathologies well before their histological manifestation.

Discussion

The previous research from our group showed that HFD-fed SAMP6 mice become obese and develop type 2 diabetes, consistent with the onset of metabolic syndrome [9]. The HFD-fed mice also developed markedly enlarged fatty livers, suggesting that they might serve as a good murine model for NAFLD. Livers from HFD-fed mice demonstrated simple steatosis and inflammation, but little DNA damage, suggesting pathological changes consistent with NAFLD fatty liver that had not completely transitioned to NASH [31]. RNASeq studies were largely confirmatory, showing an up-regulation of genes encoding proteins associated with the complement pathway and immune responses, and down-regulation of those associated with metabolic processes [32–34, 43]. Although histological examination of HFD-fed mouse fatty livers did not exhibit evidence of fibrosis or cancer, bioinformatic approaches applied to transcriptional analysis revealed pre-fibrotic and premalignant transcriptional signatures that were absent in the RNA of LFD-fed mice. These findings suggest that the pathogenesis of both fibrosis and cancer may initiate in fatty livers transitioning to NASH well before associated histological changes are evident. These data suggest that genomic changes driving disease progression toward cirrhosis and hepatocellular carcinoma may be initiated at a very early stage in fatty livers that have not completely transitioned to NASH.

Comparison of the results of the current study with other studies in the literature is complicated by the use of different diets and different mouse strains. In particular, the balance between fat and carbohydrate contents of different

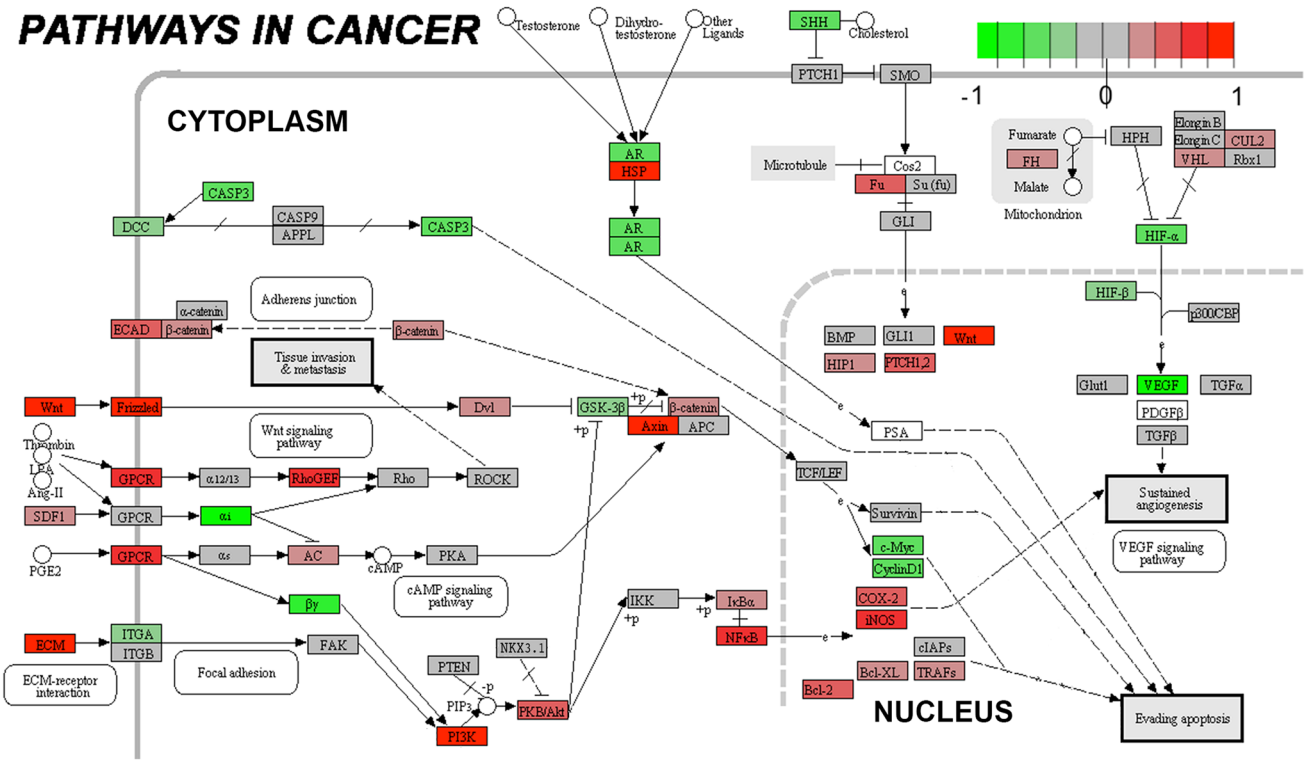

Fig. 6 Fatty livers demonstrate a premalignant signature. KEGG pathway analysis of pathways in cancer demonstrates up-regulation of multiple cancer-related growth factor receptors, growth factors, heat shock proteins, and signaling proteins (red) in the livers of HFD-fed, but not LFD-fed, mice despite the lack of histopathological evidence of carcinoma in corresponding liver tissues. Gene expression levels are indicated as significantly higher (red), unchanged (gray), or lower (green) in HFD-fed compared to LFD-fed mice

mouse chows may account for some of the similarities and differences in liver pathology and RNA signatures observed between studies. For example, Kristiansen et al. [44] detailed that C57Bl/6J mice fed the high-fat, high-carbohydrate (40% kcal from each) AMylin Liver Nash Model (AMLN) diet for 26 weeks developed liver disease consistent with nonalcoholic steatohepatitis (NASH), e.g., the mouse liver tissues demonstrated high levels of steatosis (score 3) and stage 1–3 fibrosis. RNASeq analysis revealed differential gene expression signatures consistent with elevated inflammatory response pathways, expression of multiple collagen types, and decreased metabolic pathways, similar to the transcript profiles observed in the study reported here. However, Kristiansen et al. [44] did not report transcript signatures suggestive of association with growth factor pathways or with the transformed phenotype in the AMLN diet-fed mice. The Kristiansen et al. study determined that AMLN mice evinced an elevation in plasma insulin levels of about threefold compared to lean chow-fed mice, but this difference was not statistically significant and was not accompanied by differences in fasting blood glucose levels [44]. Thus, unlike the HFD-fed mice utilized in the current study, the AMLN-fed mice did not develop a phenotype consistent with type 2 diabetes. Another study exclusively examined the role(s) of type 2 diabetes in the development of liver pathobiology. This study, by Zhang et al. [45], examined the RNA signature of liver tissues from db/db mice, who developed a syndrome similar to type 2 diabetes. Liver tissues from these mice exhibited down-regulation of genes that encode proteins associated with the immune response (including many of the complement genes) and an up-regulation of genes associated with metabolic processes [45]. Some genes associated with hepatocellular carcinoma were up-regulated, though a pro-fibrotic signature was not detected [45]. Notably, the db/db mice were not fed a high-fat diet and did not develop fatty liver. In contrast, the SAMP6 HFD-fed mice developed both type 2 diabetes [9] and fatty liver. Studies by Kristiansen et al. [44] and Zhang et al. [45] suggest that the up-regulation of immune response transcripts and down-regulation of metabolic function transcripts is likely associated more with the intake of high-fat rather than high-carbohydrate diets, though the use of different mouse strains (C57Bl/6, db/db, and SAMP6) in those and the current study likely contribute to the observed differences in liver pathobiologies as well.

Unlike either the Kristiansen et al. [44] or Zhang et al. [45] studies, the current study detected a premalignant RNA signature in HFD-fed mouse fatty livers. Studies by Shen et al. [46] showed that induction of hepatocellular carcinoma

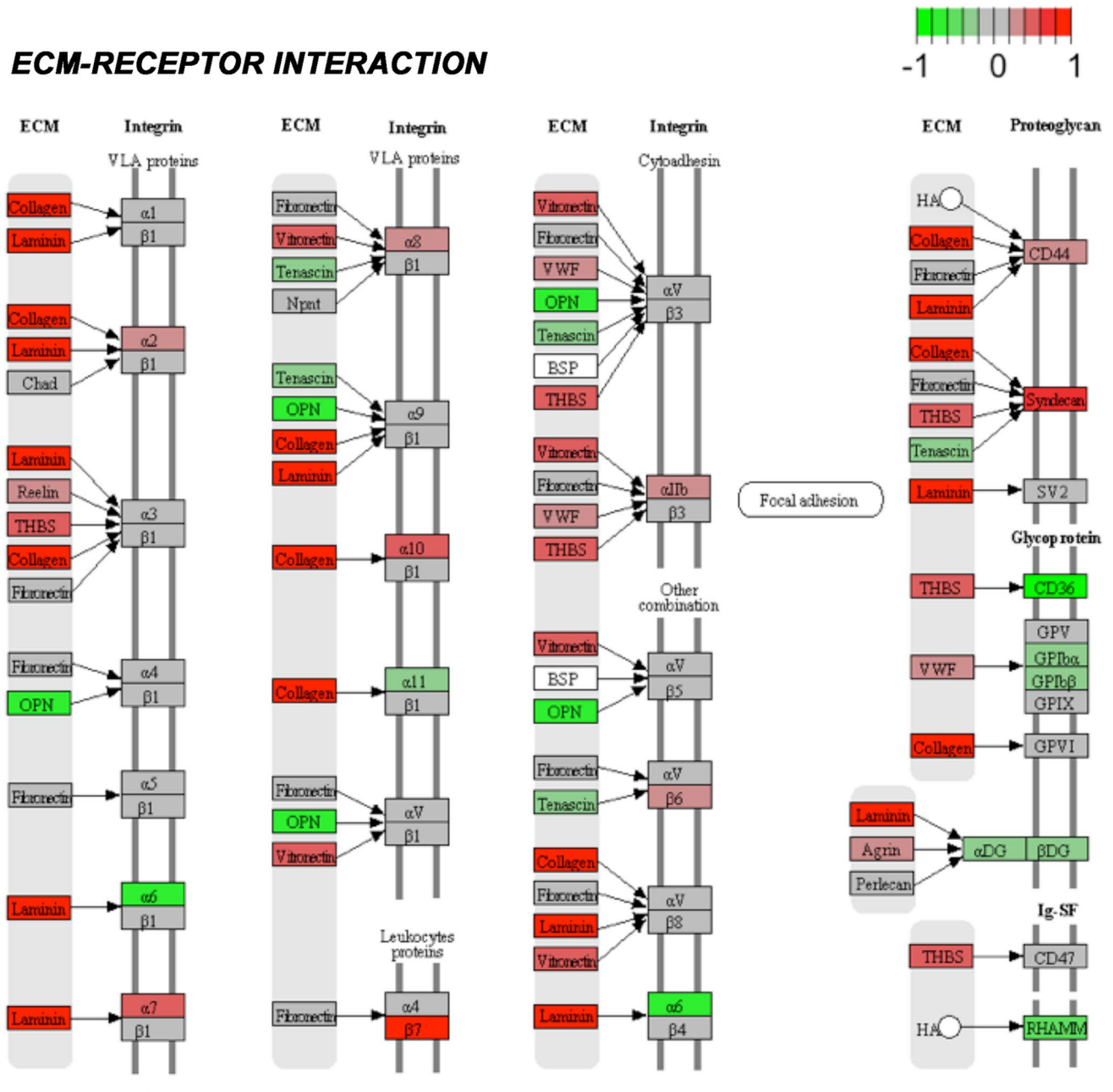

Fig. 7 Fatty livers demonstrate a pre-fibrotic signature. Pathview analysis demonstrates up-regulation of genes encoding collagen and extracellular matrix-related proteins in the livers of HFD-fed, but not LFD-fed, mice despite the lack of histopathological evidence of fibrosis in corresponding liver tissues. Gene expression levels are indicated as significantly higher (red), unchanged (gray), or lower (green) in HFD-fed compared to LFD-fed mice

with the carcinogen diethylnitrosamine (DEN) was accelerated in C57BL/6 mice fed a high-fat diet compared to those fed with regular mouse chow. These studies further identified activating HRAS mutations in liver tissues of DEN-treated obese mice, which are known to stimulate kinase-mediated signaling pathways. Interestingly, the current study identified significantly elevated levels of transcripts encoding P13K/AKT signaling pathway proteins in the livers of HFD-fed mice, a finding consistent with the identification of amplification and activating mutations of PI3K and Akt genes in human NAFLD-related liver cancers [47] which has been translated to therapeutic approaches targeting PI3K/Akt signaling to treat human hepatocellular carcinoma [48]. These data suggest that the up-regulation of growth factor receptor tyrosine kinase signaling pathways in fatty liver may signal cellular changes consistent with incipient

tumorigenesis. The current study also showed that HFD-fed mice demonstrated up-regulation of genes encoding proteins in the Wnt/β-catenin signaling pathway which is known to be subject to mutation and up-regulation in ~ 50% of human hepatocellular carcinomas [49]. Genes encoding G-protein-coupled receptors (GPCRs), which promote cell survival, proliferation, invasion, metastasis, neovascularization, and cell–cell signaling contributing to hepatocellular carcinoma, often through cross-talk with PI3K and Wnt signaling pathways [50], were up-regulated in hepatic tissues from HFD-fed mice. Notably, many of the genes that were up-regulated in hepatic tissues from HFD-fed mice encode proteins that "drive" expression of the hallmarks of cancer across diverse tumor types, including (as noted above) cell proliferation, angiogenesis, PI3K/Akt signaling, and cell–cell signaling [51].

Transcriptomic data reported here identified a pre-fibrotic signature that was evident at the transcriptional, but not protein or histological, levels. Hepatic fibrosis is associated with increased levels of ECM, which include collagen, laminin, hyaluron, elastin, and fibronectin [52]. Genes encoding collagen and laminin, but not fibronectin or elastin, were up-regulated in hepatic tissues from HFD-fed mice. Taken together, these data suggest that the gene expression profile of liver tissues from HFD-fed mice displays an incipient and early, though incomplete, fibrotic signature.

Despite the use of different mouse models and dietary approaches, common themes emerge from a consideration of the studies discussed above and those reported here. Clearly, both high-fat and high-carbohydrate diets contribute to the development and progression of NAFLD. However, the combined data reported above suggest that the transition from NAFLD to NASH and to hepatocellular carcinoma may be more strongly promoted by a high-fat than high-carbohydrate diet. However, the current study suggests that high-fat diet alone may be insufficient for a complete transition from NAFLD fatty liver to NAFLD NASH. Clearly, the development and analysis of additional mouse models would be useful to better delineate these pathobiological mechanisms.

Although the present study was limited by the relatively small number of mice examined, the data show a clear distinction between HFD- and LFD-fed mice, suggesting that the major results and conclusions would not have changed significantly by including a higher number of mice in the study. Another potential limitation is the inability to carry out the study to its logical conclusion, e.g., keeping the mice on their respective diets for 12–24 months. This limitation is unavoidable, however, as the high-fat diet is intolerable over extended periods of time and can lead to acute lower urinary tract dysfunction, including acute urinary retention, which can be fatal [9].

The studies described above imply that perhaps more aggressive clinical attention and intervention may be warranted for patients with NAFLD. One recent study reached this conclusion and proposed increased clinical awareness and improved screening strategies to translate recent treatment progress into early treatment and improved quality of life for patients with type 2 diabetes and fatty liver [53]. NAFLD patients can benefit from treatment options including exercise- and dietary intervention-based lifestyle changes [54] to improve the disease biochemically and histologically. Evidence that NAFLD is now the most common cause of liver disease in children from the developed world [55] provides additional rationale for early intervention to prevent liver damage and progression to cirrhosis or carcinoma among NAFLD patients. Fortunately, the use of mouse models such as those presented here and in the studies cited above may identify molecular DNA, RNA, and protein markers that can determine the extent of liver pathobiology even in the absence of tissue histopathology. Such markers could be useful for identifying patients who may benefit from lifestyle changes to reduce liver tissue injury and help repair organ function at an early stage before irreparable damage occurs.

Summary

High-fat diet-fed SAMP6 mice develop "diabesity," characterized by concurrent obesity and metabolic syndrome, as well as markedly enlarged fatty livers, suggesting that they might serve as a good murine model for NAFLD. High-fat diet-fed SAMP6 mouse fatty livers physiologically mimic human NAFLD in that they demonstrate simple steatosis and an up-regulation of genes encoding proteins associated with the complement pathway and immune responses, and down-regulation of those associated with metabolic processes. These livers also showed pre-fibrotic and premalignant transcriptional signatures, suggesting that the pathogenesis of both fibrosis and cancer may initiate in fatty livers well before associated histological changes are evident. The use of molecular makers identified from mouse studies could be useful for identifying patients who may benefit from lifestyle changes to reduce liver tissue injury and help repair organ function at an early stage before irreparable damage occurs.

Acknowledgments Thank you to the members of the CPCT laboratory for assistance and support. Funding for this research was provided in part by the Sanofi Genzyme grant to the College of Science and Mathematics, the Massachusetts Life Science Center, and NIH/NIGMS R25 GM076321 (D.A). We thank Dana-Farber/Harvard Cancer Center in Boston, MA, for the use of the Rodent Histopathology Core, and Dr. Roderick Bronson, who provided histodiagnostic service and is supported in part by an NCI Cancer Center Support Grant # NIH 5 P30 CA06516.

Author's contribution DA and MG-K performed mouse husbandry and molecular analyses. DA, JAR-N, CC, and TR performed RNA sequencing data alignment and analyses. JAM designed and supervised the studies. Funding was provided by the Sanofi Genzyme grant to the College of Science and Mathematics, the Massachusetts Life Science Center (J.A.M.), and NIH/NIGMS R25 GM076321 (D.A). The authors have no competing interests.

Compliance with ethical standards

Conflict of interest Other than the financial support cited above, there are no further financial or other conflicts of interest to disclose.

Ethical standard This study is fully compliant with publication and institutional ethical standards.

References

1. Paschos P, Paletas K. Non alcoholic fatty liver disease and metabolic syndrome. *Hippokratia*. 2009;13:9–19.
2. Kaur J. A comprehensive review on metabolic syndrome. *Cardiol Res Pract*. 2014;2014:943162.
3. Eckel RH, Grundy SM, Zimmet PZ. The metabolic syndrome. *Lancet*. 2005;365:1415–1428.
4. Marchesini G, Brizi M, Bianchi G, et al. Nonalcoholic fatty liver disease: a feature of the metabolic syndrome. *Diabetes*. 2001;50:1844–1850.
5. Bedogni G, Miglioli L, Masutti F, Tiribelli C, Marchesini G, Bellentani S. Prevalence of and risk factors for nonalcoholic fatty liver disease: the Dionysos nutrition and liver study. *Hepatology*. 2005;42:44–52.
6. Katsiki N, Mikhailidis DP, Mantzoros CS. Non-alcoholic fatty liver disease and dyslipidemia: an update. *Metabolism*. 2016;65:1109–1123.
7. Hubscher SG. Histological assessment of non-alcoholic fatty liver disease. *Histopathology*. 2006;49:450–465.
8. Takeda T, Hosokawa M, Higuchi K. Senescence-accelerated mouse (SAM): a novel murine model of senescence. *Exp Gerontol*. 1997;32:105–109.
9. Gharaee-Kermani M, Rodriguez-Nieves JA, Mehra R, Vezina CA, Sarma AV, Macoska JA. Obesity-induced diabetes and lower urinary tract fibrosis promote urinary voiding dysfunction in a mouse model. *Prostate*. 2013;73:1123–1133.
10. Takeda T, Matsushita T, Kurozumi M, Takemura K, Higuchi K, Hosokawa M. Pathobiology of the senescence-accelerated mouse (SAM). *Exp Gerontol*. 1997;32:117–127.
11. Azuma K, Zhou Q, Kubo KY. Morphological and molecular characterization of the senile osteoporosis in senescence-accelerated mouse prone 6 (SAMP6). *Med Mol Morphol*. 2018;51:139–146.
12. Sugimura Y, Sakurai M, Hayashi N, Yamashita A, Kawamura J. Age-related changes of the prostate gland in the senescence-accelerated mouse. *Prostate*. 1994;24:24–32.
13. Tanisawa K, Mikami E, Fuku N, et al. Exome sequencing of senescence-accelerated mice (SAM) reveals deleterious mutations in degenerative disease-causing genes. *BMC Genom*. 2013;14:248.
14. Zhang G, Zhang B, Fu X, et al. Senescence-Accelerated Mouse (SAM) strains have a spontaneous mutation in the Abcb1a gene. *Exp Anim*. 2008;57:413–417.
15. Van Heek M, Compton DS, France CF, et al. Diet-induced obese mice develop peripheral, but not central, resistance to leptin. *J Clin Invest*. 1997;99:385–390.
16. Gharaee-Kermani M, Mehra R, Robinson DR, Wei JT, Macoska JA. Complex cellular composition of solitary fibrous tumor of the prostate. *Am J Pathol*. 2014;184:732–739.
17. Tuominen VJ, Ruotoistenmaki S, Viitanen A, Jumppanen M, Isola J. ImmunoRatio: a publicly available web application for quantitative image analysis of estrogen receptor (ER), progesterone receptor (PR), and Ki-67. *Breast Cancer Res*. 2010;12:R56.
18. Stahelin BJ, Marti U, Solioz M, Zimmermann H, Reichen J. False positive staining in the TUNEL assay to detect apoptosis in liver and intestine is caused by endogenous nucleases and inhibited by diethyl pyrocarbonate. *Mol Pathol*. 1998;51:204–208.
19. Trapnell C, Pachter L, Salzberg SL. TopHat: discovering splice junctions with RNA-Seq. *Bioinformatics*. 2009;25:1105–1111.
20. Kim D, Pertea G, Trapnell C, Pimentel H, Kelley R, Salzberg SL. TopHat2: accurate alignment of transcriptomes in the presence of insertions, deletions and gene fusions. *Genome Biol*. 2013;14:R36.
21. Mouse Genome Sequencing C, Waterston RH, Lindblad-Toh K, et al. Initial sequencing and comparative analysis of the mouse genome. *Nature*. 2002;420:520–562.
22. Trapnell C, Williams BA, Pertea G, et al. Transcript assembly and quantification by RNA-Seq reveals unannotated transcripts and isoform switching during cell differentiation. *Nat Biotechnol*. 2010;28:511–515.
23. Trapnell C, Hendrickson DG, Sauvageau M, Goff L, Rinn JL, Pachter L. Differential analysis of gene regulation at transcript resolution with RNA-seq. *Nat Biotechnol*. 2013;31:46–53.
24. Robinson MD, McCarthy DJ, Smyth GK. edgeR: a Bioconductor package for differential expression analysis of digital gene expression data. *Bioinformatics*. 2010;26:139–140.
25. Luo W, Brouwer C. Pathview: an R/Bioconductor package for pathway-based data integration and visualization. *Bioinformatics*. 2013;29:1830–1831.
26. Shannon P, Markiel A, Ozier O, et al. Cytoscape: a software environment for integrated models of biomolecular interaction networks. *Genome Res*. 2003;13:2498–2504.
27. Bindea G, Mlecnik B, Hackl H, et al. ClueGO: a Cytoscape plug-into decipher functionally grouped gene ontology and pathway annotation networks. *Bioinformatics*. 2009;25:1091–1093.
28. Falcon S, Gentleman R. Using GOstats to test gene lists for GO term association. *Bioinformatics*. 2007;23:257–258.
29. Akazawa Y, Nakao K. To die or not to die: death signaling in nonalcoholic fatty liver disease. *J Gastroenterol*. 2018;53:893–906.
30. Gadd VL, Skoien R, Powell EE, et al. The portal inflammatory infiltrate and ductular reaction in human nonalcoholic fatty liver disease. *Hepatology*. 2014;59:1393–1405.
31. Kleiner DE, Brunt EM. Nonalcoholic fatty liver disease: pathologic patterns and biopsy evaluation in clinical research. *Semin Liver Dis*. 2012;32:3–13.
32. Qin X, Gao B. The complement system in liver diseases. *Cell Mol Immunol*. 2006;3:333–340.
33. Hillebrandt S, Wasmuth HE, Weiskirchen R, et al. Complement factor 5 is a quantitative trait gene that modifies liver fibrogenesis in mice and humans. *Nat Genet*. 2005;37:835–843.

34. Rensen SS, Slaats Y, Driessen A, et al. Activation of the complement system in human nonalcoholic fatty liver disease. *Hepatology*. 2009;50:1809–1817.
35. Wlazlo N, van Greevenbroek MM, Ferreira I, et al. Activated complement factor 3 is associated with liver fat and liver enzymes: the CODAM study. *Eur J Clin Invest*. 2013;43:679–688.
36. Jia Q, Li C, Xia Y, et al. Association between complement C3 and prevalence of fatty liver disease in an adult population: a cross-sectional study from the Tianjin Chronic Low-Grade Systemic Inflammation and Health (TCLSIHealth) cohort study. *PLoS ONE*. 2015;10:e0122026.
37. Boyault S, Rickman DS, de Reynies A, et al. Transcriptome classification of HCC is related to gene alterations and to new therapeutic targets. *Hepatology*. 2007;45:42–52.
38. Kudo M. Signaling pathway/molecular targets and new targeted agents under development in hepatocellular carcinoma. *World J Gastroenterol*. 2012;18:6005–6017.
39. Komposch K, Sibilia M. EGFR signaling in liver diseases. *Int J Mol Sci*. 2015;17:30.
40. Brenner DA, Waterboer T, Choi SK, et al. New aspects of hepatic fibrosis. *J Hepatol*. 2000;32:32–38.
41. Cohen JC, Horton JD, Hobbs HH. Human fatty liver disease: old questions and new insights. *Science*. 2011;332:1519–1523.
42. Karsdal MA, Manon-Jensen T, Genovese F, et al. Novel insights into the function and dynamics of extracellular matrix in liver fibrosis. *Am J Physiol Gastrointest Liver Physiol*. 2015;308:G807–G830.
43. Parks E, Yki-Jarvinen H, Hawkins M. Out of the frying pan: dietary saturated fat influences nonalcoholic fatty liver disease. *J Clin Invest*. 2017;127:454–456.
44. Kristiansen MN, Veidal SS, Rigbolt KT, et al. Obese diet-induced mouse models of nonalcoholic steatohepatitis-tracking disease by liver biopsy. *World J Hepatol*. 2016;8:673–684.
45. Zhang F, Xu X, Zhang Y, Zhou B, He Z, Zhai Q. Gene expression profile analysis of type 2 diabetic mouse liver. *PLoS ONE*. 2013;8:e57766.
46. Shen J, Tsoi H, Liang Q, et al. Oncogenic mutations and dysregulated pathways in obesity-associated hepatocellular carcinoma. *Oncogene*. 2016;35:6271–6280.
47. Michelotti GA, Machado MV, Diehl AM. NAFLD, NASH and liver cancer. *Nat Rev Gastroenterol Hepatol*. 2013;10:656–665.
48. Gao JJ, Shi ZY, Xia JF, Inagaki Y, Tang W. Sorafenib-based combined molecule targeting in treatment of hepatocellular carcinoma. *World J Gastroenterol*. 2015;21:12059–12070.
49. Khalaf AM, Fuentes D, Morshid AI, et al. Role of Wnt/beta-catenin signaling in hepatocellular carcinoma, pathogenesis, and clinical significance. *J Hepatocell Carcinoma*. 2018;5:61–73.
50. Peng WT, Sun WY, Li XR, Sun JC, Du JJ, Wei W. Emerging roles of g protein-coupled receptors in hepatocellular carcinoma. *Int J Mol Sci*. 2018. https://doi.org/10.3390/ijms19051366.
51. Uhlen M, Zhang C, Lee S, et al. A pathology atlas of the human cancer transcriptome. *Science*. 2017. https://doi.org/10.1126/science.aan2507.
52. Lim JW, Dillon J, Miller M. Proteomic and genomic studies of non-alcoholic fatty liver disease—clues in the pathogenesis. *World J Gastroenterol*. 2014;20:8325–8340.
53. Cusi K. Treatment of patients with type 2 diabetes and non-alcoholic fatty liver disease: current approaches and future directions. *Diabetologia*. 2016;59:1112–1120.
54. Katsagoni CN, Georgoulis M, Papatheodoridis GV, Panagiotakos DB, Kontogianni MD. Effects of lifestyle interventions on clinical characteristics of patients with non-alcoholic fatty liver disease: a meta-analysis. *Metabolism*. 2017;68:119–132.
55. Mencin AA, Lavine JE. Nonalcoholic fatty liver disease in children. *Curr Opin Clin Nutr Metab Care*. 2011;14:151–157.